Radiology: Cardiothoracic Imaging

REVIEW

# 4D Flow MRI of the Thoracic Aorta

*David Dushfunian, MD*[1] • *Sebastian Cohn, BS*[1] • *Haben Berhane, MS*[1,2] • *Michael Markl, PhD*[1,2]

Author affiliations, funding, and conflicts of interest are listed at the end of this article.

*Radiology: Cardiothoracic Imaging* 2025; 7(4):e240532 • https://doi.org/10.1148/ryct.240532 • Content codes: CA MR

Four-dimensional (4D) flow MRI has emerged as a versatile technique for the three-dimensional evaluation of blood flow dynamics, offering the ability to visualize flow patterns qualitatively and allow for the retrospective quantification of standard and advanced hemodynamic parameters. Recent advancements in 4D flow MRI technology, including optimized acquisition protocols and improved hemodynamic analysis workflow efficiency, have facilitated its integration into standard clinical practice, enhancing the accessibility and applicability of this innovative imaging modality. A growing body of studies have demonstrated its clinical value for monitoring and informing the management of aortic pathologies, cementing its role in modern cardiovascular care. In this review, the authors provide a concise overview of data acquisition techniques and hemodynamics analysis methods for 4D flow MRI, with a specific focus on the thoracic aorta. The core of this article explores the clinical applications of aortic 4D flow MRI in patients with aortic valve disease, aortopathy, coarctation, dissection, connective tissue disorders, and age-related changes. Furthermore, the authors discuss the emerging role of artificial intelligence on improving 4D flow MRI acquisition and processing efficiencies.



Time-resolved three-dimensional (3D) phase-contrast MRI, known as four-dimensional (4D) flow MRI, has emerged as an important noninvasive imaging technique, offering a comprehensive evaluation of cardiovascular 3D blood flow dynamics. By enabling retrospective 3D visualization and quantification of blood flow within the heart and adjacent vessels across the entire cardiac cycle, 4D flow MRI provides important insights into both normal and pathologic cardiovascular function (1–5). Early applications of 4D flow MRI focused on diseases of the aorta, including aortic aneurysms, dissections, coarctation of the aorta (CoA), and bicuspid aortic valve (BAV) (6–12). 4D flow MRI uniquely facilitates the assessment of complex in vivo 3D hemodynamic parameters involved in pathophysiologic processes that are difficult to capture with other imaging modalities. 4D flow MRI–derived measurements of aortic hemodynamics have shown potential to act as imaging biomarkers to improve diagnostic and prognostic evaluation of aortic diseases.

Doppler echocardiography is widely used in clinical practice to assess cardiovascular blood flow, providing two-dimensional (2D) quantification of velocities and pressure gradients with the aorta (13). Similarly, 2D phase-contrast MRI offers a noninvasive means to assess aortic blood flow, particularly in deeper vascular segments that cannot easily be accessed with echocardiography. However, both modalities are limited to 2D unidirectional velocity measurements. In contrast, 4D flow MRI offers a comprehensive, time-resolved 3D assessment of complex flow patterns, enabling both qualitative and quantitative analysis. A meta-analysis of 10 studies demonstrated a stronger correlation between 4D flow MRI and echocardiography measures than that observed between 2D phase-contrast MRI and echocardiography, emphasizing its potential clinical value (14). Despite its advantages, achieving clinically acceptable acquisition and processing times remains a challenge for 4D flow MRI.

In recent years, the field of 4D flow MRI has witnessed wide adoption owing to advances in MRI hardware, data acquisition, and reconstruction techniques, as well as increased availability of commercially available postprocessing solutions. These developments have paved the way for the clinical integration of 4D flow sequences into existing standard of care protocols and adoption at many centers globally (15). This review aims to provide a concise overview of the clinical applications of 4D flow MRI in the thoracic aorta. We also highlight future directions and the potential future impact of artificial intelligence (AI) on increasing the efficiency of 4D flow MRI techniques and data analysis workflows. We would like to emphasize that this article does not provide an exhaustive review of 4D MRI methods but focuses on the most common applications within the thoracic aorta. For a more comprehensive exploration of 4D flow MRI methods and broader application areas, readers are encouraged to consult other review articles (16–18) and the 4D flow MRI consensus statements (3,15).

## 4D Flow Data Acquisition

4D flow MRI builds on acquiring data in all three velocity-encoding directions (Vx, Vy, and Vz) for a prescribed 3D imaging volume. Anatomic coverage can range from a focused volume (eg, aortic acquisition in sagittal oblique orientation) to a full coronal acquisition of the whole chest. For a typical cardiovascular 4D flow MRI sequence, the heart rate is monitored by an MRI-compatible electrocardiography to enable either prospective or retrospective cardiac gating. For each cardiac time frame, four successive acquisitions are collected: one to capture a reference (magnitude) scan, and three to acquire velocity-encoded acquisitions along the x-, y-, and z-directions. Data are acquired during free breathing with the option to use respiratory gating methods to minimize respiration artifacts. In addition to heart rate, the time it takes to acquire 4D flow MRI depends on the scan parameters selected. For example, achieving higher spatial or temporal resolution requires longer scan times. For 4D flow application in the thoracic aorta, typical scan parameters include a spatial resolution of 2.0–2.5 $mm^3$, a temporal resolution of 30–50 msec, a velocity sensitivity (venc) of 150–400 cm/sec depending on expected peak velocities, and a scan time of 5–10 minutes. Recent advancements, including imaging acceleration with parallel imaging and compressed sensing, have a high potential to further reduce scan times to 2–5 minutes

### Abbreviations

AAo = ascending aorta, AI = artificial intelligence, AS = aortic stenosis, AVR = aortic valve replacement, BAV = bicuspid aortic valve, CoA = coarctation of the aorta, FL = false lumen, 4D = four-dimensional, MFS = Marfan syndrome, PWV = pulse wave velocity, TL = true lumen, 3D = three-dimensional, 2D = two-dimensional, WSS = wall shear stress


### Summary

This review highlights selected applications and future directions of four-dimensional flow MRI in the thoracic aorta.


### Essentials

- Four-dimensional (4D) flow MRI facilitates comprehensive evaluation of thoracic aortic three-dimensional blood flow dynamics, providing both quantitative and qualitative three-dimensional insights.
- 4D flow MRI can be employed to quantify advanced hemodynamic parameters such wall shear stress, kinetic energy, and pulse wave velocity, which have shown promise in risk assessment and prognostic planning for aortic pathologies.
- Clinical studies have demonstrated the diagnostic utility of 4D flow MRI in evaluating aortic valve disease, aortopathy, coarctation, dissection, connective tissue disorders, and age-related changes.
- Ongoing advancements continue to facilitate the incorporation of 4D flow MRI into routing clinical workflows.


### Keywords

Aorta, MR-Imaging, Vascular, Aortic Valve, 4D Flow MRI, Phase-Contrast, Hemodynamics, Clinical Applications


(19,20). For an in-depth review and recommendations for clinical applications of 4D flow MRI, the reader is referred to consensus statements that have been published on this technique with details of the acquisition and analysis approach (3,15).

## Hemodynamic Quantification

4D flow MRI data acquisition results in a large series (3000–10 000) of time-resolved anatomic (magnitude) and three-directional flow (Vx, Vy, and Vz) images. As a result, data postprocessing is required, which enables retrospective visualization and quantification of blood flow parameters at any location or region in the aorta. As shown in Figure 1, this capability provides an advantage over 2D phase-contrast imaging, in which measurements are restricted to preselected planes determined by the MRI technician during scan acquisition. With 4D flow MRI, standard flow metrics such as peak velocity, net flow, and regurgitant fraction can be quantified simultaneously at multiple locations (Fig 1C). 3D visualization of 4D flow MRI data can be performed using approaches such as velocity maximum intensity projections and particle trace streamlines or pathlines. Maximum intensity projections are used to show intuitive maps of the velocity distribution (see Figs 4, 5) while streamlines and pathlines further depict the flow patterns in three dimensions and over time for detailed assessment of aortic flow patterns, including flow jets and vortical flow—features not detectable with 2D imaging (see Fig 1B).

Beyond standard flow measures, such as net flow, forward flow, reverse flow, regurgitant fraction, and peak velocity, 4D flow MRI facilitates the derivation of advanced hemodynamic parameters, including but not limited to wall shear stress (WSS), pulse wave velocity (PWV), turbulent kinetic energy, viscous energy loss, pressure gradients, helicity, and vorticity. A summary of these advanced hemodynamics metrics is provided in Table 1. Advanced parameters from 4D flow MRI require additional analysis and are an ongoing area of research. Several candidates have emerged as promising measures for clinical application, as highlighted below.

## 4D Flow MRI Thoracic Aorta Applications

Over the past decade, 4D flow MRI has become more widely available by all main manufacturers of MRI scanners. In addition, 4D flow MRI analysis tools are now commercially available. This has led to an increased use of this technique both for research studies and in clinical practice. The aim of this section is to present a nonexhaustive review of selected 4D flow MRI applications in the thoracic aorta. Table 2 summarizes key studies and references regarding the applications of 4D flow MRI in aortic valve disease and aortopathy, aortic dissection, CoA, connective tissue disease, and aging.

### Aortic Valve Disease and Aortopathy

4D flow MRI has emerged as a valuable tool for assessing the aortic valve, offering comprehensive, 3D, and time-resolved insights into hemodynamics. Unlike echocardiography and 2D phase-contrast imaging, which typically provide single-directional flow data, 4D flow MRI captures multidirectional flow dynamics. This capability enables precise retrospective velocity measurements and detailed characterization of blood flow patterns, which are critical for risk assessment and prognostic planning.

BAV is the most congenital aortic valve abnormality, affecting 1%–2% of the U.S. population, and is strongly associated with increased risk of ascending aorta (AAo) dilatation, aneurysm, and dissection. Research using 4D flow MRI has provided significant insights into the pathophysiologic mechanisms underlying aortopathy in patients with BAV. Early studies demonstrated abnormal flow patterns, including elevated WSS, which is implicated in vascular remodeling (10,11,42). Later studies confirmed that patients with BAV exhibit altered flow patterns and significantly higher peak velocities and WSS compared with age- and sex-matched controls (43,44). Figure 2 provides an example comparing a normal control tricuspid aortic valve with a patient with BAV and associated aortic stenosis (AS) and dilatation. The example clearly shows marked flow jets at the right anterior aortic wall indicating high aortic shear stress with associated abnormal vortical flow patterns compared with the control. Valve morphology and fusion type have also been shown to contribute to the heterogeneity of flow patterns, WSS distributions, and expression of aortopathy in BAV (10,45). Rodríguez-Palomares et al (46) showed that right-left BAV morphology is associated with higher axial WSS at the aortic root whereas right-left morphology has higher circumferential WSS in mid and distal AAo. Further, Dux-Santoy et al (47) showed that right-noncoronary fusion type is associated with AAo dilatation. These findings underscore the utility of 4D flow MRI in differentiating patterns of aortopathy in patients with BAV.

4D flow MRI is particularly useful in studying AS because it allows for precise adaptation of the valve analysis plane across

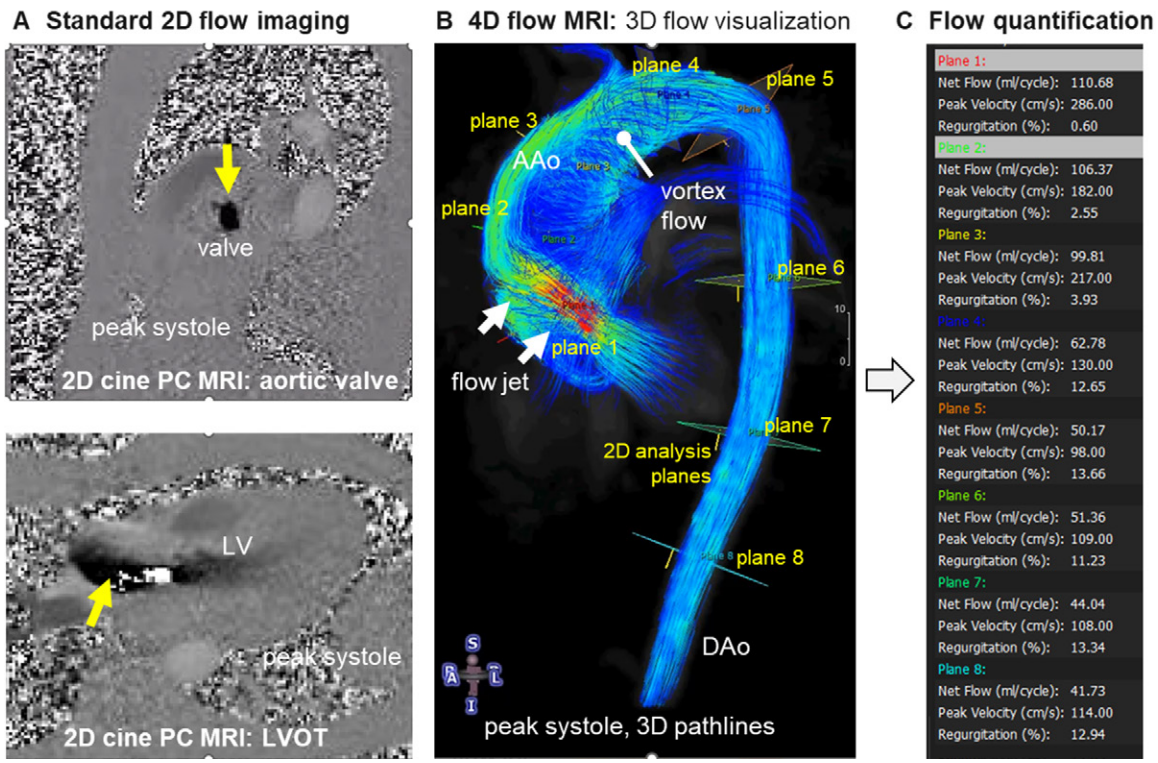


**Figure 1:** Standard two-dimensional (2D) flow imaging and four-dimensional (4D) flow MRI in a patient with bicuspid aortic valve disease and aortic valve stenosis. **(A)** Standard 2D flow imaging at the level of the aortic valve (through-plane velocity encoding) and in the left ventricular out flow tract (LVOT, in-plane velocity encoding) shows high systolic velocities and velocity aliasing distal to the narrowed aortic valve (yellow arrows). **(B)** Aortic 4D flow MRI can provide additional information over 2D flow imaging, including the three-dimensional (3D) blood flow visualization of aortic flow patterns such as a marked systolic valve flow jet (white arrows) and pronounced vortex flow in the distal ascending aorta (AAo). **(C)** 4D flow MRI allows for retrospective quantification of aortic velocities and flow using 2D analysis planes at any location along the aorta whereas 2D flow analysis is limited to the location that was selected by the MRI technologist during the MRI examination. DAo = descending aorta, LV = left ventricle, PC = phase contrast.

the cardiac cycle, accommodating valve motion. AS has been linked to higher pressure gradients compared with healthy controls, with the greatest pressure drops observed in the descending aorta in patients with moderate to severe AS (48). Studies have also demonstrated elevated WSS in patients with AS, with the degree of elevation correlating with AS severity (11,49). Notably, elevated WSS has been associated with elastic fiber thinning of the aorta medial wall, highlighting the role of hemodynamics in the development of aortic wall degeneration and aortopathy (50). These findings emphasize the utility of 4D flow MRI in detecting hemodynamic changes and their pathologic consequences.

Aortic aneurysms are often asymptomatic, with over 95% of thoracic aneurysms remaining silent until catastrophic events like rupture or dissection occur (51). Current monitoring approaches rely primarily on aortic diameter measurements to track disease progression (52). However, diameter alone is an imprecise predictor because aneurysm rupture or dissection can occur even within a normal range. 4D flow MRI provides enhanced insights into aortic physiology, combining qualitative assessments (eg, helicity, vorticity) with quantitative metrics (eg, peak velocity, WSS, oscillatory shear index) that extend beyond simple diameter evaluation. Abnormal blood flow, such as vortex formation, has been significantly correlated with increasing AAo diameter. Additionally, reduced systolic WSS and elevated oscillatory shear index are strongly associated with aortic dilatation (53). Similarly, infrarenal aneurysms exhibit disturbed flow patterns characterized by reduced WSS and elevated oscillatory shear index, which may contribute to aneurysm progression (54).

The development of WSS heat maps has further advanced the evaluation of aortic pathologies. These maps quantify areas of elevated or reduced (outside 95% CIs of normal values) WSS compared with normal population averages, accounting for age and sex differences (55,56). Guzzardi et al (57) showed significant associations between elevated WSS areas (>95% of normal values), aorta wall extracellular matrix degradation, and elastic fiber degradation on histopathology in patients with BAV. Figure 3A highlights these associations between areas of elevated WSS on heat maps and extracellular matrix remodeling. Kiema et al (58) also showed the relationship between increased WSS and medial degeneration. Soulat et al (59) used WSS heat maps to follow patients with BAV over more than 5 years to monitor progressive aortic dilatation (Fig 3B). The study showed that areas of elevated WSS significantly correlated with higher rates of aortic dilatation compared with age- and sex-matched controls. It is noteworthy that these findings have been verified independently by two other groups, providing strong evidence that hemodynamics assessment by 4D flow has a high potential to contribute to improved management of patients with aortic valve disease and aortopathy (60,61).

## Aortic Dissection

Aortic dissection is a life-threatening condition characterized by an intimal tear in the aorta, resulting in the formation of a

**Table 1: Standard and Advanced 4D Flow MRI Hemodynamic Measures**

| Hemodynamic Measure | Description | Reference |
|---|---|---|
| Standard measures | | |
| Peak velocity (m/sec) | Highest speed of blood flow measured within a particular region or vessel over a given time period (eg, systole). | (21,22) |
| Net flow (mL/min) | The total flow (sum of forward and reverse flow) through the vessel. | (23–25) |
| Peak flow (mL/sec) | Maximum volume of blood passing through a region over a given time period (eg, systole). | (23,24) |
| Regurgitant fraction (%) | Proportion of blood flow backward relative to the forward flow. | (26,27) |
| Advanced measures | | |
| WSS (Pa) | Shear forces of blood acting tangentially on the vessel wall. WSS is a biomarker for endothelial dysfunction and vessel remodeling attributed to aberrant blood flow. WSS can be reported as absolute numbers (eg, systolic WSS magnitude) or decomposed into axial and circumferential components. | (28,29) |
| PWV (m/sec) | Propagation speed of blood pressure pulse through vessels. PWV is an indicator of vessel wall elasticity and stiffness. | (30,31) |
| TKE (J) | Energy dissipation associated with turbulent blood flow. TKE can be an indicator of blood flow efficiency. | (32,33) |
| Viscous energy loss (J) | Energy lost due to viscous friction of different layers of blood flow | (34,35) |
| Pressure gradient (mm Hg) | Pressure changes across a valve or aortic region. The gradient is an indicator of stenosis severity whether across the aortic valve or coarctation. | (36,37) |
| Helicity ($m/sec^2$) | Corkscrew forward motion of blood along the vessel. Helicity provides information of the complex blood flow patterns that may impact vessel wall function. | (38,39) |
| Vorticity (1/sec) | Local spinning of blood flow creating a swirl within the flow. Vorticity can be used to grade complex blood flow derangements in conditions such as aneurysm, aortic valve stenosis, or coarctation. | (40,41) |

Note.—4D = four-dimensional, PWV = pulse wave velocity, TKE = turbulent kinetic energy, WSS = wall shear stress.

true lumen (TL) and a false lumen (FL) within the vessel wall. Traditionally, aortic diameter has been the primary parameter for risk stratification and guiding the timing of interventions. However, 4D flow MRI can provide additional hemodynamic insights that complement anatomic data, enhancing the accuracy of patient risk assessment. Notably, 4D flow MRI enables clear differentiation between the TL and FL (62) and offers valuable insights into interactions between the TL and FL, including metrics such as relative pressure and the FL ejection fraction (the ratio of blood exiting the FL to that in the TL during diastole). These parameters have been identified as significant predictors of aortic growth rate (63,64). Moreover, 4D flow MRI can identify hemodynamically active fenestrations, which may predispose the aorta to rupture or further dilatation (65). Figure 4 illustrates a 4D flow MRI–derived systolic velocity maximum intensity projection, clearly depicting discrete fenestrations between the TL and FL in a patient with aortic dissection. Takahashi et al (66) linked specific FL blood flow characteristics, such as nonlaminar flow driven by high velocity and volume, to an elevated risk of complications, emphasizing the impact of 4D flow data on patient outcomes.

Additionally, 4D flow MRI–derived quantification of flow energetics in the TL and FL have been associated with adverse outcomes. Chu et al (67) demonstrated that the FL/TL kinetic energy ratio could predict aortic growth, with adverse outcomes correlating with lower FL reverse flow, increased FL stasis, and reduced TL kinetic energy, forward flow, and peak velocity. Jarvis et al (68) analyzed aortic flow patterns in patients with repaired type A dissections and those with medically managed descending aorta dissections. Their findings revealed that patients with repaired type A dissection exhibited elevated TL reverse flow and kinetic energy compared with controls and higher TL and FL kinetic energy with lower FL stasis compared with patients with descending aorta dissection.

These findings highlight the potential of 4D flow MRI as a transformative tool for risk assessment and prognostic planning in the management of aortic dissection. By integrating hemodynamic and anatomic data, 4D flow MRI could enhance clinical decision-making and support personalized treatment strategies.

## Aortic Coarctation

CoA is a condition characterized by narrowing of the aortic lumen, typically congenital but occasionally acquired. Its management traditionally relies on invasive catheterization to assess systolic pressure gradients. Recent advances have demonstrated the potential of 4D flow MRI as a noninvasive alternative for evaluating flow changes and pressure gradients in CoA. Saitta et al (69) validated 4D flow–derived pressure fields against patient-specific fluid–structure interaction models, demonstrating strong concordance between MRI-derived data and computational simulations. Accurate pressure measurement is vital for monitoring disease progression in CoA, and Riesenkampff et

**Table 2: Literature on 4D Flow MRI–derived Flow Measures in Aortic Valve Disease and Aortopathy, Aortic Dissection, CoA, Connective Tissue Disease, and Aging**

| Literature | No. of Participants | Key Finding |
|---|---|---|
| Aortic valve disease and aortopathy | | |
| Bissell et al (11) | 142 | Patients with BAV with AS had higher values of WSS and increased WSS eccentricity. |
| Meierhofer et al (43) | 18 | Patients with BAV with no valve or vessel disease have higher WSS in the AAo than age- and sex-matched controls. |
| Allen et al (44) | 30 | In pediatric and young adult patients with BAV, AS, and AAo PV are associated with increased AAo WSS. |
| Mahadevia et al (10) | 75 | Type and morphology of BAV leaflets are associated with abnormal flow patterns, changes in WSS distribution, and aortopathy phenotype. |
| Barker et al (45) | 60 | Patients with BAV have asymmetric increased WSS compared with controls with TAV. WSS is associated with AAo flow jet pattern, which is influenced by BAV fusion pattern. |
| Rodríguez-Palomares et al (46) | 131 | Right-left BAV morphology is associated with higher axial WSS at the aortic root whereas right-noncoronary has a higher circumferential WSS in mid and distal AAo. |
| Dux-Santoy et al (47) | 156 | In-plane rotational flow, right-noncoronary BAV, and systolic flow reversal ratio are predictors of aortic dilatation. |
| Fatehi Hassanabad et al (48) | 43 | Patients with BAV have higher pressure drops than healthy controls. Moderate to severe stenosis is associated with higher pressure drops at the descending segments. |
| Farag et al (49) | 73 | Increased AAo WSS in patients with BAV depends on the presence of AS. Aortic dilatation is most pronounced with the presence of AS and nondilated AAo. |
| Bollache et al (50) | 47 | Increased WSS is associated with elastic fiber thinning in patients with BAV. |
| Bürk et al (53) | 63 | AAo dilatation is associated with reduced WSS and increased oscillatory shear index. |
| Takehara et al (54) | 18 | Infrarenal aortic aneurysms exhibit disturbed flow patterns, with dilated regions displaying lower WSS and higher oscillatory shear index. |
| Guzzardi et al (57) | 20 | AAo regions with increased WSS show extracellular matrix dysregulation and elastic fiber degradation in patients with BAV. |
| Kiema et al (58) | 32 | Aortic regions with increased WSS are associated with medial degeneration and thinning. |
| Soulat et al (59) | 72 | Patients with BAV with larger areas of elevated WSS in AAo and entire aorta have higher rates of AAo dilatation (>0.24 mm/y) over time (OR = 1.51 and 1.71, respectively). |
| Guala et al (60) | 47 | Circumferential WSS is positively correlated with AAo growth rates in patients with BAV. |
| Minderhoud et al (61) | 60 | WSS angle is associated with aortic growth in patients with BAV. |
| Shan et al (120) | 65 | AS or insufficiency results in elevated WSS and flow eccentricity. |
| van Ooij et al (121) | 571 | BAV with AS is associated with elevated WSS. Cusp fusion phenotypes result in distinct WSS distributions. TAV with aortic dilatation is associated with lower WSS. |
| Shan et al (122) | 140 | Severe AS exacerbates aortic flow aberrations in patients with BAV. |
| Weiss et al (123) | 655 | Systolic RF is elevated in patients with BAV compared with patients with TAV with aortic dilatation. AS and AR severity contribute to the extent of systolic RF. |
| Dissection | | |
| Marlevi et al (63) | 12 | FL ejection fraction and relative pressure correlated with aortic growth rates ($r$ = 0.78 and −0.64, respectively) and are independent predictors of growth. |
| Burris et al (64) | 18 | FL ejection fraction is an independent predictor of aortic growth rate after adjusting for covariates (β =.15, $P$ = .004). |
| Allen et al (65) | 19 | 4D flow MRI improves detection of hemodynamically active dissection flaps and reentry tear sites. |
| Takahashi et al (66) | 33 | High-volume turbulent flow in the FL is associated with increased risk of late complications (rupture or intervention). |
| Chu et al (67) | 51 | FL/TL KE ratio is a possible predictor of aortic growth. Adverse outcomes correlated with lower FL-RF, FL stasis, TL-KE, TL-FF and TL-PV. |

***(Table 2 continues)***

**Table 2 (*continued*): Literature on 4D Flow MRI–derived Flow Measures in Aortic Valve Disease and Aortopathy, Aortic Dissection, CoA, Connective Tissue Disease, and Aging**

| Literature | No. of Participants | Key Finding |
|---|---|---|
| Jarvis et al (68) | 55 | Patients with repaired type A aortic dissection have elevated TL-RF and TL-KE compared with controls and higher TL and FL KE and lower FL-stasis compared with patients with DAo dissection. |
| Allen et al (124) | 53 | FL ejection fraction is an independent predictor of aorta-related adverse outcomes. Entry tear net flow is associated with aortic growth rates. |
| Engel et al (125) | 32 | Longitudinal TL and FL hemodynamic changes are associated with aortic growth rates in patients with type B aortic dissection. |
| Coarctation | | |
| Riesenkampff et al (70) | 13 | 4D flow MRI–derived pressure fields have excellent correlation and agreement ($r$ = 0.86–0.97) with invasive catheterization at five aortic locations. |
| Hope et al (71) | 34 | Patients after a successful CoA surgical correction demonstrate normal blood flow velocity profiles. |
| Soulat et al (72) | 15 | Increased baseline PV at the CoA site is associated with progressive narrowing after repair ($r$ = −0.64; $P$ = .010). |
| Desai et al (126) | 99 | Patients with CoA have higher peak velocities and WSS in the arch and DAo and flow derangements in the DAo compared with controls. |
| Rengier et al (127) | 26 | Pressure difference amplitudes and spatial pressure range at mid systole are significantly increased in patients with repaired CoA compared with volunteers in the arch, proximal DAo, and the distal DAo. |
| Connective tissue disease | | |
| Geiger et al (73) | 36 | Patients with MFS had lower peak systolic velocities, decreased net flow per cycle, and higher circumferential WSS compared with controls. |
| van der Palen et al (74) | 46 | Patients with MFS have reduced WSS in the proximal AAo and proximal DAo as well as higher WSS in the inner segment of the distal AAo compared with controls. |
| Guala et al (75) | 234 | Patients with MFS have increased PWV compared with participants with TAV. |
| Westenberg et al (76) | 50 | PWV is higher in all parts of the aorta in patients with MFS compared with healthy volunteers. |
| Kröner et al (77) | 47 | Regional PWV is significantly increased in patients with MFS compared with healthy volunteers. PWV has moderate to high specificity for predicting absence of regional aortic luminal growth. |
| Leidenberger et al (78) | 22 | Patients with MFS have reduced aortic distensibility and increased midsystolic pressure gradient in the proximal AAo, which correlated with larger aortic root diameter. |
| Geiger et al (128) | 29 | Patients with MFS have lower WSS and increased localized aberrant vortex/helix flow patterns at the inner proximal DAo segment, which correlates with enlarged diameter at critical sites for aortic dissection. |
| Aging | | |
| Callaghan and Grieve (79) | 224 | WSS decreases significantly with age. |
| Scott et al (80) | 100 | Systolic velocity and WSS changes significantly with age but not with sex. |
| Wu et al (81) | 82 | Aortic peak velocities decrease with age in adults. |
| Ebel et al (82) | 86 | WSS and maximum forward velocity of helices decrease with age. No link between age and sex was observed for WSS, helical flow, and flow jet. |
| Jarvis et al (83) | 99 | PWV increases with age, by approximately 1 m/sec per decade. Increased PWV was associated with a decline in cardiac function and reduced aortic blood flow velocity. |
| Dyverfeldt et al (85) | 46 | Tortuosity increases with age and is associated with helicity. Helicity is in turn associated with decreasing turbulent KE in different aortic regions ($\rho$ = ±0.45 to ±0.72, $P$ < .05). |
| Ha et al (86) | 42 | Turbulent blood flow develops in the aorta of healthy participants and is impacted by age-related geometric changes. |

***(Table 2 continues)***

**Table 2 (*continued*): Literature on 4D Flow MRI–derived Flow Measures in Aortic Valve Disease and Aortopathy, Aortic Dissection, CoA, Connective Tissue Disease, and Aging**

| Literature | No. of Participants | Key Finding |
|---|---|---|
| Other applications | | |
| Zhang et al (89) | 52 | PWV >6.4 m/sec could detect patients with active Takayasu disease with an AUC of 0.732 and a sensitivity of 86.67%. |
| Righini et al (94) | 10 | 4D flow MRI can detect velocity, WSS, and blood flow pattern alterations in patients after TEVAR. |
| Cosset et al (95) | 7 | In patients after TEVAR, FF increased by 21% within the TL and decreased by 13% in the FL. RF increased by 6% in the TL and decreased by 6% in the FL. |
| Katahashi et al (97) | 155 | 4D flow MRI analysis of type 2 endoleak vessels could predict sac expansion with a sensitivity of 85.7% and a specificity of 76.2%. |
| Lenz et al (98) | 20 | Patients exhibit significant reduction in aortic valve regurgitation, PV, vertical flow, helical flow, flow displacement, and WSS after aortic valve repair. |
| Keller et al (99) | 20 | Aortic root replacement reduces aberrant aortic hemodynamics and flow patterns. |
| Bissell et al (100) | 90 | Blood flow patterns normalize and WSS decreases after AVR or Ross procedure. |
| Kamada et al (101) | 10 | Aortic volume flow rate increases with a decrease in flow complexity proximal to the arch branches after AVR. |
| Bollache et al (102) | 33 | WSS decreased after AVR in at-risk regions. WSS distal to aortic root graft increased postoperatively. |
| Semaan et al (103) | 23 | Blood flow eccentricity and helicity decreased after aortic root replacement. |
| Collins et al (104) | 37 | Valve-sparing aortic root replacement resulted in improved hemodynamic outcomes compared with replacement with bioprosthetic valves. |
| Farag et al (105) | 24 | WSS and PV are higher in patients following transcatheter AVR compared with age- and sex-matched controls. |

Note.—AAo = ascending aorta, AR = aortic regurgitation, AS = aortic stenosis, AUC = area under the receiver operating characteristic curve, AVR = aortic valve replacement, BAV = bicuspid aortic valve, CoA = coarctation of the aorta, DAo = descending aorta, FF = forward flow, FL = false lumen, 4D = four-dimensional, KE = kinetic energy, MFS = Marfan syndrome, OR = odds ratio, PV = peak velocity, PWV = pulse wave velocity, RF = reverse flow, TAV = tricuspid aortic valve, TEVAR = thoracic endovascular aortic repair, TL = true lumen, WSS = wall shear stress.

al (70) found significant correlations ($r$ = 0.86–0.97) between 4D flow MRI–derived pressure fields and catheter-based measurements across five aortic sites, underscoring its potential to replace invasive methods for follow-up in patients with CoA.

4D flow MRI has also proven valuable in assessing CoA following surgical repair. Hope et al (71) showed that successful repair restored normal blood flow velocity profiles. Furthermore, 4D flow MRI identified patients at a higher risk of recoarctation. For instance, a longitudinal study by Soulat et al (72) revealed a correlation between peak velocity and reduced aortic diameter at the former coarctation site, suggesting a predisposition for renarrowing.

Additionally, 4D flow MRI–derived pathlines and streamlines provide a deeper understanding of coarctation severity and abnormal flow patterns, offering insights into disease progression and individual risk. Figure 5 illustrates aortic hemodynamics in a 60-year-old female patient with CoA. 3D flow visualization reveals areas of high velocity at the coarctation site, followed by complex and helical flow distal to the stenosis. Although 3D flow visualization with pathlines and streamlines may be subject to interobserver variability due to their qualitative nature, quantitative metrics such as vorticity, turbulent kinetic energy, and viscous energy loss can offer more objective and reproducible assessments.

## Connective Tissue Disorders of the Aorta

Aortic dilatation, particularly at the root, is a common feature in patients with connective tissue disorders such as Marfan syndrome (MFS), posing a high risk for serious complications such as aortic dissection or rupture. Studies have demonstrated altered flow patterns and hemodynamics in patients with MFS, including lower peak velocities, reduced net flow per cardiac cycle, and abnormal WSS distribution compared with healthy controls (73,74). Notably, circumferential WSS—associated with aortic growth rates—has been shown to be elevated in patients with MFS relative to controls (73).

van der Palen et al (74) identified localized helical flow in the AAo of pediatric patients with MFS, which correlated with dilatation of the sinus of Valsalva. These patients also exhibited segmental variations in WSS, with increased WSS in the distal AAo and reduced WSS in the proximal AAo and proximal descending aorta—regions commonly predisposed to aneurysmal dissection or rupture in MFS.

The abnormal connective tissue in MFS contributes to reduced aortic distensibility, reflected in elevated PWV compared with controls with tricuspid aortic valves (75–78). Kröner et al (77) demonstrated that PWV has moderate to high specificity (78%) for predicting the absence of regional aortic luminal growth,

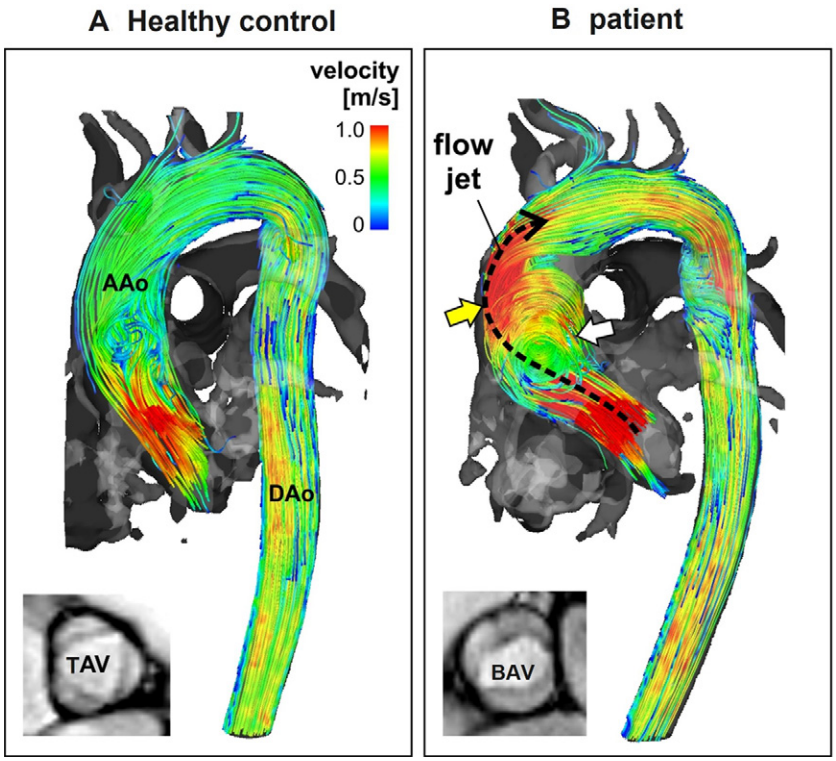


**Figure 2:** Images show four-dimensional (4D) flow MRI–derived systolic three-dimensional (3D) blood flow patterns in **(A)** a healthy participant with a tricuspid aortic valve (TAV) compared with **(B)** a patient with a bicuspid aortic valve (BAV) with aortic dilatation. For BAV, a marked flow jet (yellow arrow) impacts the right anterior aorta wall, indicating aortic regions exposed to elevated wall shear stress and at risk for aortic remodeling. Additional vortex flow is frequently observed in these patients (white arrow). AAo = ascending aorta, DAo = descending aorta.

potentially aiding in risk stratification. However, although PWV may help rule out aortic growth, Leidenberger et al (78) showed that pressure gradients in the AAo positively correlate with aortic growth rates, highlighting their prognostic value.

These findings illustrate the utility of 4D flow MRI in detecting early abnormal hemodynamics in high-risk patients. By providing detailed insights into flow and aortic mechanics, this technique has potential to support more precise management strategies and prognostic planning for patients with MFS.

## Age-related Changes in Aortic Hemodynamics

4D flow MRI is a valuable tool for tracking hemodynamic changes associated with aging. Multiple studies have demonstrated age-related decreases in WSS and aortic velocities (79–82). Ebel et al (82) reported a decline in the maximum forward velocity of helices with age and also found no significant association between sex and WSS, helical flow, or flow jets. Jarvis et al (83) investigated PWV in the thoracic aorta across adulthood, noting a consistent increase of approximately 1 m/sec per decade. This progression enabled the classification of adulthood into three distinct stages, each characterized by significantly different PWV values. A similar age–PWV trend was also observed whether aorta-targeted or whole-heart 4D flow MRI scans were used (84). Aging has also been linked to changes in blood flow patterns and aortic geometry. Dyverfeldt et al (85) observed increased aortic tortuosity with age, which was correlated with elevated helicity. Furthermore, helicity was inversely associated with turbulent kinetic energy in various aortic regions ($\rho = \pm 0.45$ to $\pm 0.72$, $P < .05$). Similarly, Ha et al (86) demonstrated a relationship between age-related morphologic changes and the development of turbulent blood flow in the AAo. Older individuals exhibited increased turbulent kinetic energy in the AAo, which was associated with age-related aortic dilatation. These findings underscore the potential of 4D flow MRI for the early detection of age-related aortic hemodynamic changes for timely preventative interventions.

## Other Applications

The utility of 4D flow MRI in the thoracic aorta extends beyond previously discussed applications, offering comprehensive hemodynamic assessment across various aortic pathologies. This imaging modality has shown to provide diagnostic value in assessing inflammatory aortic diseases, including Behçet disease, giant cell arteritis, Takayasu arteritis, and IgG4-related disease. These conditions compromise the aortic medial layer, leading to wall thickening, reduced elasticity, stenosis, and aneurysm formation (87). By providing hemodynamic information on velocity, WSS, and PWV, 4D flow MRI facilitated the identification of regions affected by aorta wall thickening, dilatation, or ulceration. Álvarez Vázquez et al (88) demonstrated its utility in qualitative and quantitative blood flow assessment in a patient with Takayasu arteritis. They used 4D flow MRI data to detect active aortic regurgitation and simultaneously assess for anomalous flows like interventricular communication. Zhang et al (89) further reported the potential role of PWV as an indicator of active aortic inflammatory process in patients with Takayasu disease. They showed that PWV was elevated in patients with active Takayasu disease compared with those with inactive disease (in remission). They also identified a diagnostic cutoff of PWV of 6.4 m/sec above which patients are deemed to have active Takayasu disease (area under receiver operating characteristic curve: 0.732, sensitivity: 86.67%). Because early detection of active inflammatory processes in Takayasu disease is crucial for management and prognosis, 4D flow provides a significant advantage over brachial-ankle and carotid-femoral PWV, which may be unreliable in patients with stenotic or occlusive peripheral artery disease.

Beyond inflammatory conditions, 4D flow MRI has been applied in the postoperative surveillance following thoracic endovascular aortic repair, in which long-term monitoring for complications such as endoleaks and stent migration is essential (90). Hope et al (91) first proposed its use in assessing type 1 endoleaks, and subsequent studies confirmed that stent grafts do not obstruct flow measurements after thoracic endovascular aortic repair (92,93). A pilot study in 10 patients revealed postoperative alterations in aortic WSS and flow patterns, with vortical and helical

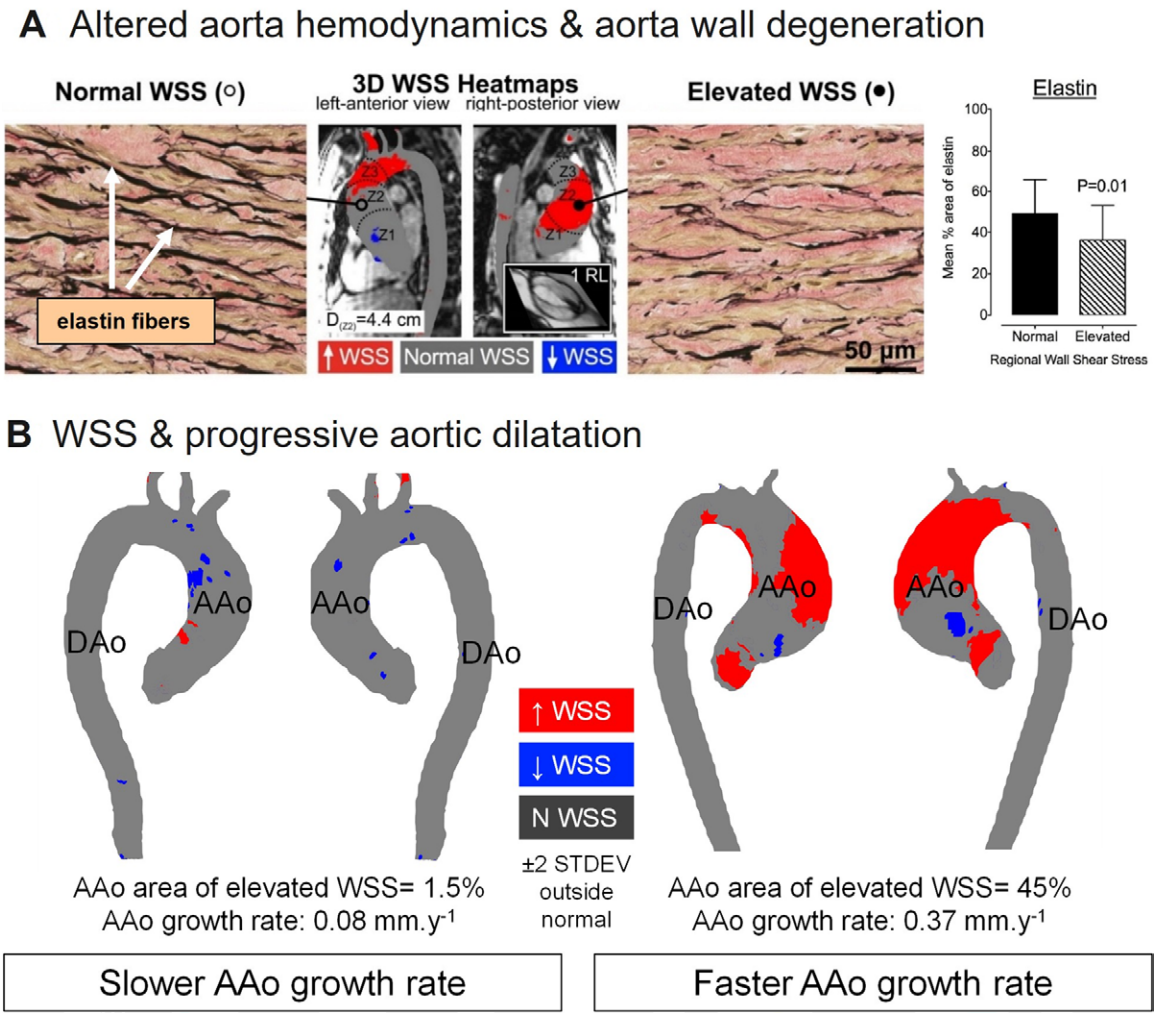


**Figure 3:** **(A)** Histopathologic images show wall shear stress (WSS)–mediated tissue dysfunction in bicuspid aortic valve (BAV). In paired aortic wall samples (elevated vs normal WSS on heat maps), regions of increased WSS show greater medial elastin degradation compared with areas with normal WSS: decreased total elastin ($P = .01$) with thinner fibers ($P < .001$). **(B)** Four-dimensional (4D) flow MRI–based WSS assessment in two patients with BAV disease. WSS heat maps show regions of elevated WSS (red) compared with age- and sex-matched control populations, demonstrating that elevated WSS in the ascending aorta is associated with progressive aortic dilatation. AAo = ascending aorta, DAo = descending aorta.

flow changes observed after thoracic endovascular aortic repair (94). Cosset et al (95) quantified flow redistribution, reporting a 21% increase in forward flow within the TL and a 13% decrease in the FL, along with corresponding reverse flow changes of +6% in the TL and −6% in the FL. Additionally, Sakata et al (96) demonstrated that 4D flow MRI was more sensitive than CT angiography in detecting type 2 endoleaks and provided further subclassification. Notably, 4D flow MRI has also been shown to predict sac expansion after endovascular repair, with a sensitivity of 85.7% and specificity of 76.2% (97).

4D flow MRI provides detailed perioperative hemodynamic analysis following aortic valve replacement (AVR) and repair, offering insights into pre- and postinterventional flow patterns, pressure gradients, and WSS dynamics. Lenz et al (98) reported that after aortic valve repair, patients exhibit reductions in aortic regurgitation, peak systolic velocity, WSS, vortical flow, helical flow, and flow displacement. In addition, helical and vortical flow abnormalities normalized after AVR, resembling healthy volunteer flow patterns. Although transvalvular pressure gradients remained elevated compared with healthy individuals, a postinterventional decrease was observed (99). Bissell et al (100) showed that flow abnormalities in patients with BAV improved following mechanical AVR or Ross procedures, with significant reductions for in-plane WSS. Additional studies demonstrated reduced post-AVR WSS in the AAo, decreased flow complexity, and increased total flow volume, particularly in the AAo and its branches (101,102). For valve-sparing aortic root repair, postoperative normalization of flow eccentricity, reduced AAo helicity, and lower aortic root velocity have been reported (103,104), although WSS may increase in regions distal to the graft (102). WSS and peak velocity have been shown to be higher in patients following transcatheter AVR compared with age- and sex-matched controls (105). In addition, 4D flow accurately quantified paravalvular regurgitation in patients with transcatheter AVR with comparable results to 2D flow acquisition (106). Figure 6 illustrates pre- and postinterventional peak velocity maximum intensity projections and WSS vector fields maps in a 52-year-old male patient who underwent aortic valve repair with aortic root replacement. The effect of intervention on aortic hemodynamics can clearly be appreciated by a marked reduction in postsurgical AAo peak velocity (2.52 m/

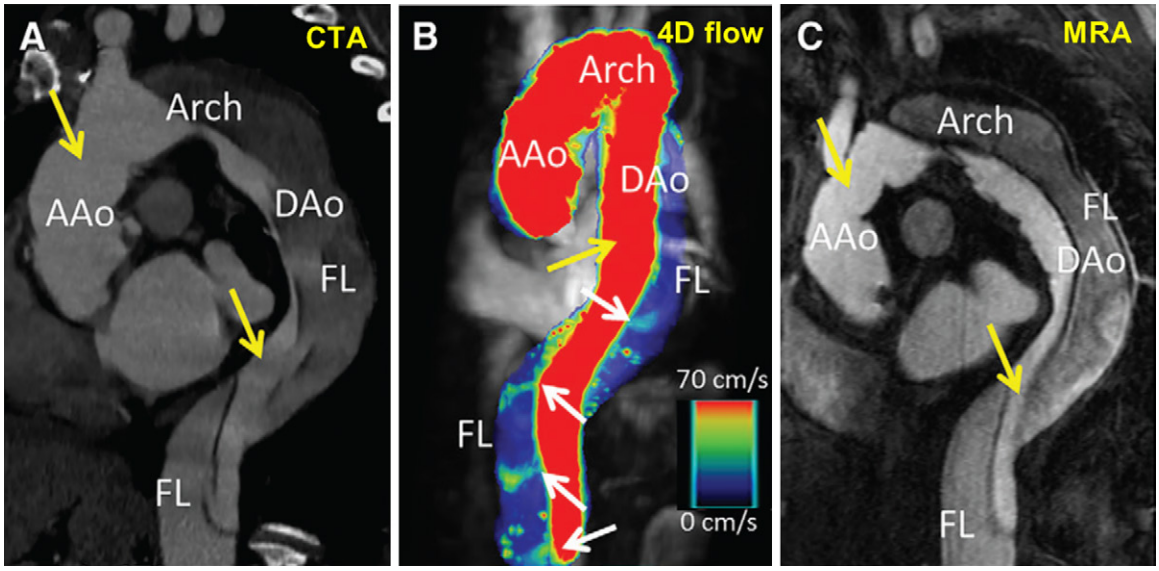


**Figure 4:** **(A)** CT angiogram (CTA), **(B)** oblique sagittal four-dimensional (4D) flow MRI velocity maximum intensity projection (MIP) image overlaid on magnitude images, and **(C)** contrast-enhanced MR angiogram (MRA) show the thoracic aorta. CTA and MRA depict dissection anatomy but both were limited by blurring artifact related to pulsatile flap motion. The 4D flow velocity MIP image reveals four discrete fenestrations from their associated flow jets into the false lumen during systole (white arrows). Yellow arrows indicate the true lumen. AAo = ascending aorta, Arch = aortic arch, DAo = descending aorta, FL = false lumen. (Reprinted, with permission, from reference 65.)

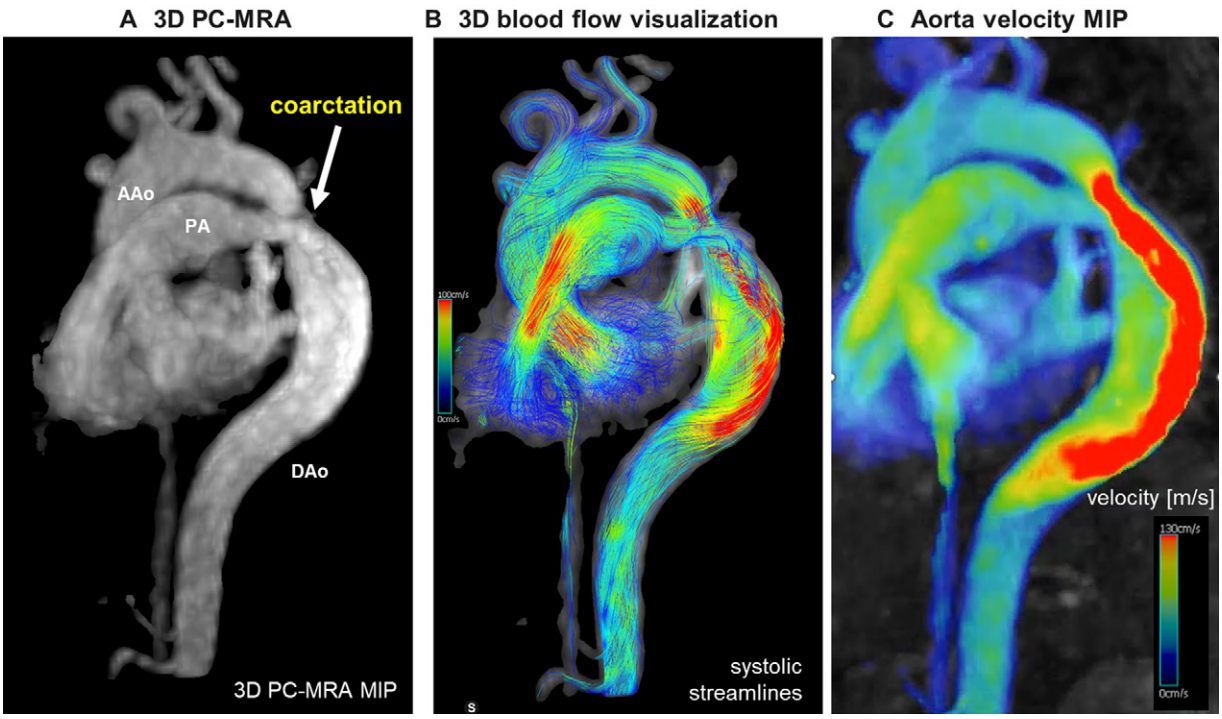


**Figure 5:** Aortic four-dimensional (4D) flow MRI in a 60-year-old female patient after repair for aortic coarctation and restenosis illustrates the comprehensive anatomic and hemodynamic information that can be derived from a single 4D flow MRI. **(A)** 4D flow–derived three-dimensional (3D) phase-contrast (PC) MR angiogram (MRA) data show aortic anatomy. **(B)** Systolic streamlines illustrate 3D flow patterns, including high flow velocities at and distal to the coarctation. **(C)** Peak systolic velocity maximum intensity projection (MIP) provides intuitive maps of the velocity distribution across the aorta and can be used to identify abnormal flow patterns such a regional of marked flow acceleration. Further, velocity MIPs can guide the optimal placement of two-dimensional analysis planes, as in this case to measure peak velocity at the coarctation. AAo = ascending aorta, DAo = descending aorta, PA = pulmonary artery.

sec vs 1.91 m/sec), pressure gradient (12 mm Hg vs 8 mm Hg), and regurgitation fraction (52% vs 18%). Similarly, mean and maximum WSS decreased with apparent visible changes on the WSS vector fields.

These findings highlight the role of 4D flow MRI as a noninvasive imaging tool for disease surveillance, diagnosis, and prognosis in patients with thoracic aortic pathology. By integrating blood flow assessment into clinical and postoperative management,

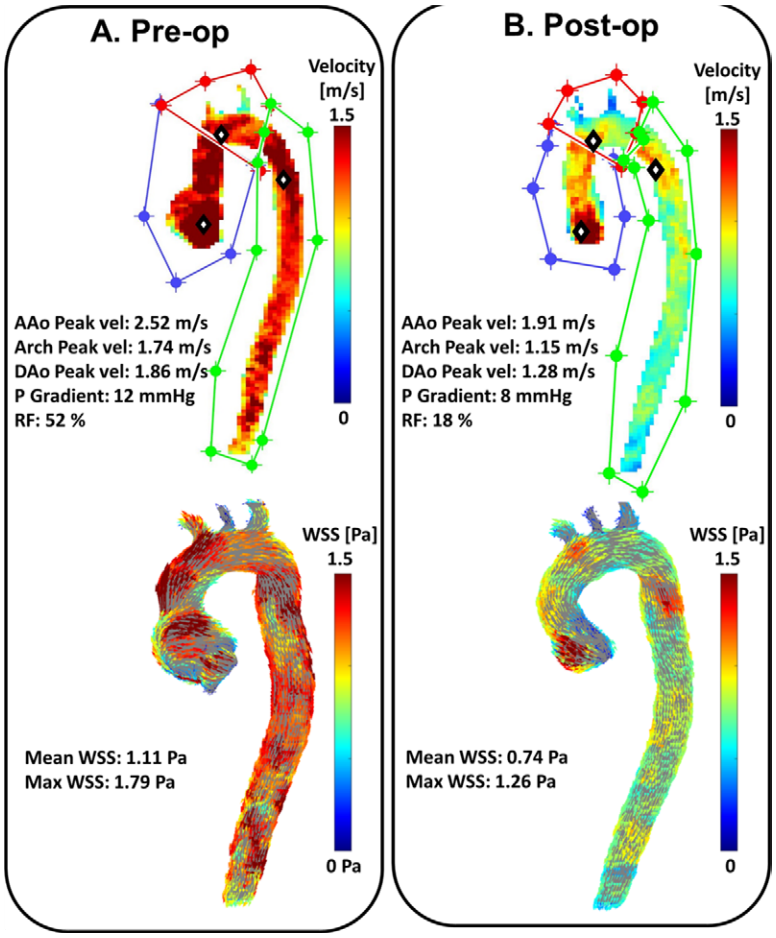


**Figure 6:** Aortic four-dimensional (4D) flow MRI in a 52-year-old male patient with bicuspid aortic valve **(A)** before and **(B)** after aortic valve repair and valve-sparing aortic root replacement illustrates hemodynamic changes postoperatively. Peak velocity maximal intensity projections (MIPs) and wall shear stress (WSS) vector fields are illustrated. Evident decrease was observed in ascending aorta (AAo) peak velocity, pressure gradient, and regurgitation fraction (RF). Similarly, mean and maximum WSS decreased postoperatively.

clinicians can enhance risk stratification, optimize prognostic planning, and improve patient outcomes.

## Future Directions and the Impact of AI

In the past years, advancements have been made to enhance 4D flow MRI by leveraging deep learning and AI. These innovations aim to address various challenges across postprocessing, reconstruction, and acquisition stages.

Although 4D flow data analysis workflow has undergone substantial improvements, including commercially available software solutions by multiple vendors, manual interaction with the data is often still needed. More recently, new deep learning analysis methods have been introduced that have a high potential to further simplify and accelerate analysis workflows. Several studies have demonstrated the efficacy of deep learning in automating and improving the analysis of aortic 4D flow MRI. For instance, Berhane et al (107) used over 1000 4D flow MRI datasets to automate the 3D segmentation of the thoracic aorta, achieving a median Dice score of over 0.95. Their method exhibited excellent agreement in net flow, peak flow, and peak velocity compared with manual segmentation. Figure 7 demonstrates an example of the AI-driven analysis providing accurate aortic segmentations, aortic diameter measurements, and blood flow quantifications compared with manual derived estimates. They further developed a convolutional neural network that effectively corrects velocity aliasing in 4D flow MRI, outperforming conventional algorithms in speed and accuracy in detecting aliased voxels (108). Bustamante et al (109) created a convolutional neural network for automatic time-resolved segmentation of major arteries in 4D flow MRI, achieving an average Dice score of 0.91 and strong to excellent agreement in hemodynamic comparisons with atlas-based segmentation. Similarly, one study used a dense encoder–decoder network (Dense-U-Net) to automatically segment the aorta from 4D flow MRI magnitude data, achieving better performance than atlas-based segmentation model (110). Physics-informed neural networks have been shown to be effective for postprocessing 4D flow measurements in an in vitro axis-symmetric stenosis (111). The neural network enabled displacement error correction, data denoising, and identifying unknown quantities. Ericsson et al (112) used ensemble learning to accurately predict high-resolution velocities from low-resolution input data in silico. This approach enabled the generation of superresolution 4D flow MRI data from downsampled in vivo data (112). Levilly et al (113) also used deep learning to develop a Segmentation-Free Super-Resolution algorithm able to efficiently compute superresolved velocity vectors from 4D flow MRI data within 10 minutes. The algorithm incorporated Navier-Stokes equations and velocity smoothing constraints to ensure realistic, reliable, and segmentation-free approach (113). Callmer et al (114) implemented a residual network (redesigned 4DFlowNet) to generate temporal superresolution 4D flow MRI. The network synthesized high-resolution temporal information from unseen in silico and in vivo data. Strong correlation was observed for in vivo data at peak flow frames. This enabled high frame rate flow quantification from low temporal resolution data, allowing acquisition times beyond clinically acceptable limits (114). Finally, Berhane et al (115) developed a robust fluid physics–informed cycle generative adversarial network that can derive systolic aortic hemodynamics from anatomic input in under 1 second without any boundary conditions. The network was trained on 1765 4D flow MRI datasets including patients with BAV and tricuspid aortic valve. 3D aortic segmentations served as the only input to derive peak systolic velocities. The deep learning model achieved strong agreement between AI and standard 4D flow MRI peak velocities ($r^2$ = 0.930–0.957, $P$ < .001), WSS (mean percentage difference = 6.2%–8.5%), and aortic valve stenosis severity classification (85.8% accuracy and $\kappa$ = 0.8). The network demonstrated the potential for substantial 4D flow MRI workflow improvement compared with standard techniques that can take 10–25 minutes (115).

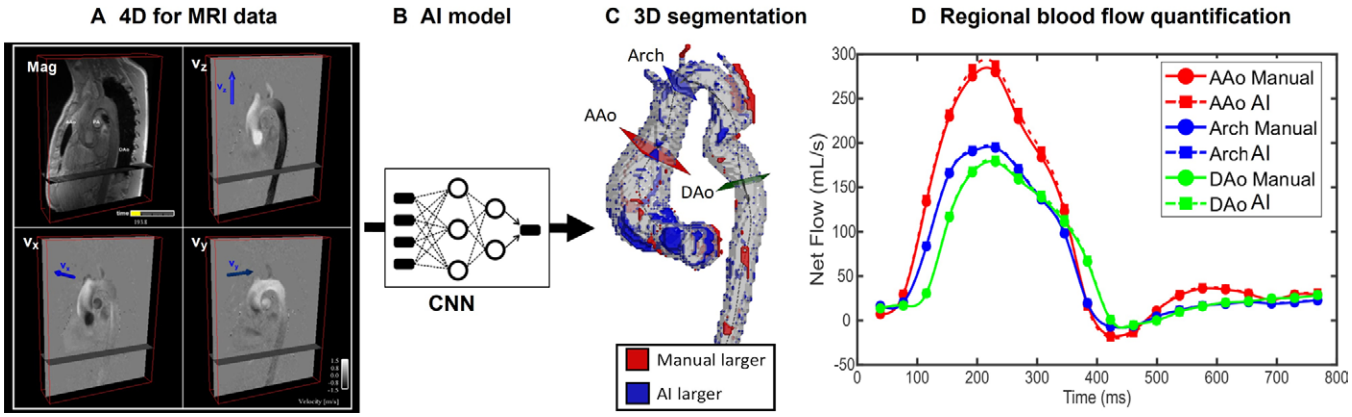


**Figure 7:** Artificial intelligence (AI)–driven four-dimensional (4D) flow MRI analysis. A deep learning network was used for fully automated and fast 4D flow MRI–based three-dimensional (3D) segmentation of the aorta and subsequent two-dimensional (2D) planar flow analysis. **(A)** 4D flow MRI input data. **(B)** Convolutional neural network (CNN) for automated 3D segmentation of the aorta. **(C)** Aorta 3D segmentation difference map (AI vs manual) and three 2D analysis planes used for quantification of flow in the ascending aorta (AAo), arch, and descending aorta (DAo). **(D)** Flow waveforms for each of the three planes (solid lines, manual 3D aorta segmentation; dashed lines, AI 3D segmentation) demonstrate excellent agreement for AI versus human 4D flow analysis.

For improving 4D flow MRI acquisitions, Vishnevskiy et al (116) introduced a deep variational network (FlowVN) designed for rapid reconstruction of highly accelerated 4D flow MRI scans, completing the process in under 1 minute. Their approach demonstrated excellent correlation in aortic flow and velocities with compressed sensing reconstruction and yielded strong structural similarity index values for reconstructed anatomic images. The same group later proposed a self-supervised reconstruction network (FlowMRI-Net) for fast reconstruction of highly undersampled 4D flow MRI data (117). The FlowMRI-Net outperformed a state-of-the-art compressed sensing and FlowVN network for aortic 4D flow MRI reconstruction with times ranging between 1 and 7 minutes on commodity central processing unit and graphics processing unit hardware. Further, Kim et al (118) proposed a three-point velocity encoding strategy to accelerate 4D flow MRI. This technique captures the three velocity-encoded scans ($V_x$, $V_y$, $V_z$) without the need for a reference scan, using a convolutional neural network for background phase removal. This innovative method has the potential to accelerate 4D flow MRI by up to 25% and can be integrated with other acceleration techniques to further minimize scan times.

These developments suggest a promising future for 4D flow MRI, driven by deep learning technologies that enhance clinical feasibility through reduced scan times and improved efficiency of hemodynamic analysis workflows. To further integrate 4D flow MRI into clinical practice, future AI models will be required to be reliable, generalizable, and efficient, with validation against reference-standard techniques. It will be crucial to move beyond single-source, black-box approaches. Instead, AI models should incorporate prior knowledge and constraints—such as embedding Navier-Stokes equations in velocity data generation—and leverage multivendor, multisite datasets from diverse patient populations to ensure interpretability and trustworthiness (119). AI-driven models have the potential to enhance every aspect of cardiac MRI, from protocol optimization and scanning to data acquisition, reconstruction, and analysis. This increased automation will enable more frequent use of 4D flow MRI, facilitating timely diagnosis, surveillance, and prognostic planning. Ultimately, these advancements will support radiographers and physicians in collecting and analyzing critical data, leading to improved patient outcomes.

## Conclusion

4D flow MRI has emerged as a noninvasive imaging technique, allowing for comprehensive post hoc assessments of 3D blood flow and imaging biomarkers in the heart and great vessels. Its ability to provide both quantitative and qualitative analyses of blood flow offers significant advantages over traditional methods like 2D phase-contrast MRI and echocardiography. Clinical studies highlight its utility in evaluating the thoracic aorta, aiding in risk stratification and management of aortic conditions. Recent advancements in postprocessing techniques, reduced scan times, and the availability of user-friendly analysis packages have facilitated broader clinical adoption of 4D flow MRI. Looking ahead, the integration of deep learning and AI aims to automate analysis workflows and provide immediate blood flow quantifications, enhancing the clinical applicability of this innovative technique.

**Author affiliations:**

[1] Department of Radiology, Feinberg School of Medicine, Northwestern University; 737 N Michigan Ave, Ste 1600, Chicago, IL 60611

[2] Department of Biomedical Engineering, McCormick School of Engineering, Northwestern University, Evanston, Ill

Received December 4, 2024; revision requested February 10, 2025; final revision received June 11; accepted July 9.

**Address correspondence to:** M.M. (email: mmarkl@northwestern.edu).

**Disclosures of conflicts of interest: D.D.** No relevant relationships. **S.C.** No relevant relationships. **H.B.** No relevant relationships. **M.M.** Grants from Siemens, Circle Cardiovascular Imaging; president of the Society for Cardiovascular Magnetic Resonance (SCMR); co-founder of Third Coast Dynamics; associate editor of *Radiology: Cardiothoracic Imaging*.

## References

1. Markl M, Frydrychowicz A, Kozerke S, Hope M, Wieben O. 4D flow MRI. J Magn Reson Imaging 2012;36(5):1015–1036.
2. Markl M, Kilner PJ, Ebbers T. Comprehensive 4D velocity mapping of the heartand great vessels by cardiovascular magnetic resonance. J Cardiovasc Magn Reson 2011;13(1):7–22.

3. Dyverfeldt P, Bissell M, Barker AJ, et al. 4D flow cardiovascular magnetic resonance consensus statement. J Cardiovasc Magn Reson 2015;17(1):72.
4. Uribe S, Beerbaum P, Sørensen TS, Rasmusson A, Razavi R, Schaeffter T. Four-dimensional (4D) flow of the whole heart and great vessels using real-time respiratory self-gating. Magn Reson Med 2009;62(4):984–992.
5. Stankovic Z, Allen BD, Garcia J, Jarvis KB, Markl M. 4D flow imaging with MRI. Cardiovasc Diagn Ther 2014;4(2):173–192.
6. Malek AM, Alper SL, Izumo S. Hemodynamic shear stress and its role in atherosclerosis. JAMA 1999;282(21):2035–2042.
7. Hope MD, Hope TA, Crook SES, et al. 4D flow CMR in assessment of valve-related ascending aortic disease. JACC Cardiovasc Imaging 2011;4(7):781–787.
8. Hope MD, Hope TA, Meadows AK, et al. Bicuspid aortic valve: four-dimensional MR evaluation of ascending aortic systolic flow patterns. Radiology 2010;255(1):53–61.
9. Silber HA, Bluemke DA, Ouyang P, Du YP, Post WS, Lima JA. The relationship between vascular wall shear stress and flow-mediated dilation: endothelial function assessed by phase-contrast magnetic resonance angiography. J Am Coll Cardiol 2001;38(7):1859–1865.
10. Mahadevia R, Barker AJ, Schnell S, et al. Bicuspid aortic cusp fusion morphology alters aortic three-dimensional outflow patterns, wall shear stress, and expression of aortopathy. Circulation 2014;129(6):673–682.
11. Bissell MM, Hess AT, Biasiolli L, et al. Aortic dilation in bicuspid aortic valve disease: flow pattern is a major contributor and differs with valve fusion type. Circ Cardiovasc Imaging 2013;6(4):499–507.
12. den Reijer PM, Sallee D 3rd, van der Velden P, et al. Hemodynamic predictors of aortic dilatation in bicuspid aortic valve by velocity-encoded cardiovascular magnetic resonance. J Cardiovasc Magn Reson 2010;12(1):4.
13. Nishimura RA, Otto CM, Bonow RO, et al. AHA/ACC guideline for the management of patients with valvular heart disease: a report of the American College of Cardiology/American Heart Association Task Force on Practice Guidelines. J Am Coll Cardiol 2014;63(22):e57–e185.
14. Xu K, Wang XD, Yang ZG, et al. Quantification of peak blood flow velocity at the cardiac valve and great thoracic vessels by four-dimensional flow and two-dimensional phase-contrast MRI compared with echocardiography: a systematic review and meta-analysis. Clin Radiol 2021;76(11):863.e1–863.e10.
15. Bissell MM, Raimondi F, Ait Ali L, et al. 4D Flow cardiovascular magnetic resonance consensus statement: 2023 update. J Cardiovasc Magn Reson 2023;25(1):40.
16. Takahashi K, Sekine T, Ando T, Ishii Y, Kumita S. Utility of 4D flow MRI in thoracic aortic diseases: a literature review of clinical applications and current evidence. Magn Reson Med Sci 2022;21(2):327–339.
17. Garcia J, Barker AJ, Markl M. The role of imaging of flow patterns by 4D flow MRI in aortic stenosis. JACC Cardiovasc Imaging 2019;12(2):252–266.
18. Catapano F, Pambianchi G, Cundari G, et al. 4D flow imaging of the thoracic aorta: is there an added clinical value? Cardiovasc Diagn Ther 2020;10(4):1068–1089.
19. Huang F, Akao J, Vijayakumar S, Duensing GR, Limkeman M. k-t GRAPPA: A k-space implementation for dynamic MRI with high reduction factor. Magn Reson Med 2005;54(5):1172–1184.
20. Ma LE, Markl M, Chow K, et al. Aortic 4D flow MRI in 2 minutes using compressed sensing, respiratory controlled adaptive k-space reordering, and inline reconstruction. Magn Reson Med 2019;81(6):3675–3690.
21. Nordmeyer S, Riesenkampff E, Messroghli D, et al. Four-dimensional velocity-encoded magnetic resonance imaging improves blood flow quantification in patients with complex accelerated flow. J Magn Reson Imaging 2013;37(1):208–216.
22. Rose MJ, Jarvis K, Chowdhary V, et al. Efficient method for volumetric assessment of peak blood flow velocity using 4D flow MRI. J Magn Reson Imaging 2016;44(6):1673–1682.
23. Bollache E, van Ooij P, Powell A, Carr J, Markl M, Barker AJ. Comparison of 4D flow and 2D velocity-encoded phase contrast MRI sequences for the evaluation of aortic hemodynamics. Int J Cardiovasc Imaging 2016;32(10):1529–1541.
24. Markl M, Wallis W, Harloff A. Reproducibility of flow and wall shear stress analysis using flow-sensitive four-dimensional MRI. J Magn Reson Imaging 2011;33(4):988–994.
25. van Ooij P, Powell AL, Potters WV, Carr JC, Markl M, Barker AJ. Reproducibility and interobserver variability of systolic blood flow velocity and 3D wall shear stress derived from 4D flow MRI in the healthy aorta. J Magn Reson Imaging 2016;43(1):236–248.
26. Hsiao A, Tariq U, Alley MT, Lustig M, Vasanawala SS. Inlet and outlet valve flow and regurgitant volume. may be directly and reliably quantified with accelerated, volumetric phase-contrast MRI. J Magn Reson Imaging 2015;41(2):376–385.
27. Feneis JF, Kyubwa E, Atianzar K, et al. 4D flow MRI quantification of mitral and tricuspid regurgitation: reproducibility and consistency relative to conventional MRI. J Magn Reson Imaging 2018;48(4):1147–1158.
28. Stalder AF, Russe MF, Frydrychowicz A, Bock J, Hennig J, Markl M. Quantitative 2D and 3D phase contrast MRI: optimized analysis of blood flow and vessel wall parameters. Magn Reson Med 2008;60(5):1218–1231.
29. Bieging ET, Frydrychowicz A, Wentland A, et al. In vivo three-dimensional MR wall shear stress estimation in ascending aortic dilatation. J Magn Reson Imaging 2011;33(3):589–597.
30. Markl M, Wallis W, Brendecke S, Simon J, Frydrychowicz A, Harloff A. Estimation of global aortic pulse wave velocity by flow-sensitive 4D MRI. Magn Reson Med 2010;63(6):1575–1582.
31. Wentland AL, Wieben O, François CJ, et al. Aortic pulse wave velocity measurements with undersampled 4D flow-sensitive MRI: comparison with 2D and algorithm determination. J Magn Reson Imaging 2013;37(4):853–859.
32. Dyverfeldt P, Kvitting JPE, Sigfridsson A, Engvall J, Bolger AF, Ebbers T. Assessment of fluctuating velocities in disturbed cardiovascular blood flow: in vivo feasibility of generalized phase-contrast MRI. J Magn Reson Imaging 2008;28(3):655–663.
33. Binter C, Knobloch V, Manka R, Sigfridsson A, Kozerke S. Bayesian multipoint velocity encoding for concurrent flow and turbulence mapping. Magn Reson Med 2013;69(5):1337–1345.
34. Barker AJ, van Ooij P, Bandi K, et al. Viscous energy loss in the presence of abnormal aortic flow. Magn Reson Med 2014;72(3):620–628.
35. Elbaz MSM, van der Geest RJ, Calkoen EE, et al. Assessment of viscous energy loss and the association with three-dimensional vortex ring formation in left ventricular inflow: In vivo evaluation using four-dimensional flow MRI. Magn Reson Med 2017;77(2):794–805.
36. Ha H, Kvitting JP, Dyverfeldt P, Ebbers T. Validation of pressure drop assessment using 4D flow MRI-based turbulence production in various shapes of aortic stenoses. Magn Reson Med 2019;81(2):893–906.
37. Falahatpisheh A, Rickers C, Gabbert D, et al. Simplified Bernoulli's method significantly underestimates pulmonary transvalvular pressure drop. J Magn Reson Imaging 2016;43(6):1313–1319.
38. Gallo D, Steinman DA, Bijari PB, Morbiducci U. Helical flow in carotid bifurcation as surrogate marker of exposure to disturbed shear. J Biomech 2012;45(14):2398–2404.
39. Lorenz R, Bock J, Barker AJ, et al. 4D flow magnetic resonance imaging in bicuspid aortic valve disease demonstrates altered distribution of aortic blood flow helicity. Magn Reson Med 2014;71(4):1542–1553.
40. Fenster BE, Browning J, Schroeder JD, et al. Vorticity is a marker of right ventricular diastolic dysfunction. Am J Physiol Heart Circ Physiol 2015;309(6):H1087–H1093.
41. Browning JR, Hertzberg JR, Schroeder JD, Fenster BE. 4D flow assessment of vorticity in right ventricular diastolic dysfunction. Bioengineering (Basel) 2017;4(2):30.
42. Barker AJ, Lanning C, Shandas R. Quantification of hemodynamic wall shear stress in patients with bicuspid aortic valve using phase-contrast MRI. Ann Biomed Eng 2010;38(3):788–800.
43. Meierhofer C, Schneider EP, Lyko C, et al. Wall shear stress and flow patterns in the ascending aorta in patients with bicuspid aortic valves differ significantly from tricuspid aortic valves: a prospective study. Eur Heart J Cardiovasc Imaging 2013;14(8):797–804.
44. Allen BD, van Ooij P, Barker AJ, et al. Thoracic aorta 3D hemodynamics in pediatric and young adult patients with bicuspid aortic valve. J Magn Reson Imaging 2015;42(4):954–963.
45. Barker AJ, Markl M, Bürk J, et al. Bicuspid aortic valve is associated with altered wall shear stress in the ascending aorta. Circ Cardiovasc Imaging 2012;5(4):457–466.
46. Rodríguez-Palomares JF, Dux-Santoy L, Guala A, et al. Aortic flow patterns and wall shear stress maps by 4D-flow cardiovascular magnetic resonance in the assessment of aortic dilatation in bicuspid aortic valve disease. J Cardiovasc Magn Reson 2018;20(1):28.
47. Dux-Santoy L, Guala A, Teixidó-Turà G, et al. Increased rotational flow in the proximal aortic arch is associated with its dilation in bicuspid aortic valve disease. Eur Heart J Cardiovasc Imaging 2019;20(12):1407–1417.
48. Fatehi Hassanabad A, Burns F, Bristow MS, et al. Pressure drop mapping using 4D flow MRI in patients with bicuspid aortic valve disease: A novel marker of valvular obstruction. Magn Reson Imaging 2020;65:175–182.
49. Farag ES, van Ooij P, Planken RN, et al. Aortic valve stenosis and aortic diameters determine the extent of increased wall shear stress in bicuspid aortic valve disease. J Magn Reson Imaging 2018;48(2):522–530.
50. Bollache E, Guzzardi DG, Sattari S, et al. Aortic valve-mediated wall shear stress is heterogeneous and predicts regional aortic elastic fiber thinning in bicuspid aortic valve-associated aortopathy. J Thorac Cardiovasc Surg 2018;156(6):2112–2120.e2.
51. Kuzmik GA, Sang AX, Elefteriades JA. Natural history of thoracic aortic aneurysms. J Vasc Surg 2012;56(2):565–571.
52. Davies RR, Goldstein LJ, Coady MA, et al. Yearly rupture or dissection rates for thoracic aortic aneurysms: simple prediction based on size. Ann Thorac Surg 2002;73(1):17–28.
53. Bürk J, Blanke P, Stankovic Z, et al. Evaluation of 3D blood flow patterns and wall shear stress in the normal and dilated thoracic aorta using flow-sensitive 4D CMR. J Cardiovasc Magn Reson 2012;14(1):84.

54. Takehara Y, Isoda H, Takahashi M, et al. Abnormal flow dynamics result in low wall shear stress and high oscillatory shear index in abdominal aortic dilatation: initial in vivo assessment with 4D-flow MRI. Magn Reson Med Sci 2020;19(3):235–246.
55. Bustamante M, Petersson S, Eriksson J, et al. Atlas-based analysis of 4D flow CMR: automated vessel segmentation and flow quantification. J Cardiovasc Magn Reson 2015;17:87.
56. Cibis M, Bustamante M, Eriksson J, Carlhäll CJ, Ebbers T. Creating hemodynamic atlases of cardiac 4D flow MRI. J Magn Reson Imaging 2017;46(5):1389–1399.
57. Guzzardi DG, Barker AJ, van Ooij P, et al. Valve-related hemodynamics mediate human bicuspid aortopathy: insights from wall shear stress mapping. J Am Coll Cardiol 2015;66(8):892–900.
58. Kiema M, Sarin JK, Kauhanen SP, et al. Wall shear stress predicts media degeneration and biomechanical changes in thoracic aorta. Front Physiol 2022;13:934941.
59. Soulat G, Scott MB, Allen BD, et al. Association of regional wall shear stress and progressive ascending aorta dilation in bicuspid aortic valve. JACC Cardiovasc Imaging 2022;15(1):33–42.
60. Guala A, Dux-Santoy L, Teixido-Tura G, et al. Wall shear stress predicts aortic dilation in patients with bicuspid aortic valve. JACC Cardiovasc Imaging 2022;15(1):46–56.
61. Minderhoud SCS, Roos-Hesselink JW, Chelu RG, et al. Wall shear stress angle is associated with aortic growth in bicuspid aortic valve patients. Eur Heart J Cardiovasc Imaging 2022;23(12):1680–1689.
62. Sherrah AG, Callaghan FM, Puranik R, et al. Multi-velocity encoding four-dimensional flow magnetic resonance imaging in the assessment of chronic aortic dissection. Aorta (Stamford) 2017;5(3):80–90.
63. Marlevi D, Sotelo JA, Grogan-Kaylor R, et al. False lumen pressure estimation in type B aortic dissection using 4D flow cardiovascular magnetic resonance: comparisons with aortic growth. J Cardiovasc Magn Reson 2021;23(1):51.
64. Burris NS, Nordsletten DA, Sotelo JA, et al. False lumen ejection fraction predicts growth in type B aortic dissection: preliminary results. Eur J Cardiothorac Surg 2020;57(5):896–903.
65. Allen BD, Aouad PJ, Burris NS, et al. Detection and hemodynamic evaluation of flap fenestrations in type B aortic dissection with 4D flow MRI: comparison with conventional MRI and CT angiography. Radiol Cardiothorac Imaging 2019;1(1):e180009.
66. Takahashi K, Sekine T, Miyagi Y, et al. Four-dimensional flow analysis reveals mechanism and impact of turbulent flow in the dissected aorta. Eur J Cardiothorac Surg 2021;60(5):1064–1072.
67. Chu S, Kilinc O, Pradella M, et al. Baseline 4D flow-derived in vivo hemodynamic parameters stratify descending aortic dissection patients with enlarging aortas. Front Cardiovasc Med 2022;9:905718.
68. Jarvis K, Pruijssen JT, Son AY, et al. Parametric hemodynamic 4D flow MRI maps for the characterization of chronic thoracic descending aortic dissection. J Magn Reson Imaging 2020;51(5):1357–1368.
69. Saitta S, Pirola S, Piatti F, et al. Evaluation of 4D flow MRI-based non-invasive pressure assessment in aortic coarctations. J Biomech 2019;94:13–21.
70. Riesenkampff E, Fernandes JF, Meier S, et al. Pressure fields by flow-sensitive, 4D, velocity-encoded CMR in patients with aortic coarctation. JACC Cardiovasc Imaging 2014;7(9):920–926. [Published correction appears in JACC Cardiovasc Imaging 2014;7(11):1183.]
71. Hope MD, Meadows AK, Hope TA, et al. Clinical evaluation of aortic coarctation with 4D flow MR imaging. J Magn Reson Imaging 2010;31(3):711–718.
72. Soulat G, Scott MB, Pathrose A, et al. 4D flow MRI derived aortic hemodynamics multi-year follow-up in repaired coarctation with bicuspid aortic valve. Diagn Interv Imaging 2022;103(9):418–426.
73. Geiger J, Arnold R, Herzer L, et al. Aortic wall shear stress in Marfan syndrome. Magn Reson Med 2013;70(4):1137–1144.
74. van der Palen RLF, Barker AJ, Bollache E, et al. Altered aortic 3D hemodynamics and geometry in pediatric Marfan syndrome patients. J Cardiovasc Magn Reson 2017;19(1):30.
75. Guala A, Rodriguez-Palomares J, Dux-Santoy L, et al. Influence of aortic dilation on the regional aortic stiffness of bicuspid aortic valve assessed by 4-dimensional flow cardiac magnetic resonance: comparison with Marfan syndrome and degenerative aortic aneurysm. JACC Cardiovasc Imaging 2019;12(6):1020–1029.
76. Westenberg JJM, Scholte AJHA, Vaskova Z, et al. Age-related and regional changes of aortic stiffness in the Marfan syndrome: assessment with velocity-encoded MRI. J Magn Reson Imaging 2011;34(3):526–531.
77. Kröner ESJ, Scholte AJHA, de Koning PJH, et al. MRI-assessed regional pulse wave velocity for predicting absence of regional aorta luminal growth in marfan syndrome. Int J Cardiol 2013;167(6):2977–2982.
78. Leidenberger T, Gordon Y, Farag M, et al. Imaging-based 4D aortic pressure mapping in Marfan syndrome patients: a matched case-control study. Ann Thorac Surg 2020;109(5):1434–1440.
79. Callaghan FM, Grieve SM. Normal patterns of thoracic aortic wall shear stress measured using four-dimensional flow MRI in a large population. Am J Physiol Heart Circ Physiol 2018;315(5):H1174–H1181.
80. Scott MB, Huh H, van Ooij P, et al. Impact of age, sex, and global function on normal aortic hemodynamics. Magn Reson Med 2020;84(4):2088–2102.
81. Wu C, Honarmand AR, Schnell S, et al. Age-related changes of normal cerebral and cardiac blood flow in children and adults aged 7 months to 61 years. J Am Heart Assoc 2016;5(1):e002657.
82. Ebel S, Kühn A, Aggarwal A, et al. Quantitative normal values of helical flow, flow jets and wall shear stress of healthy volunteers in the ascending aorta. Eur Radiol 2022;32(12):8597–8607.
83. Jarvis K, Scott MB, Soulat G, et al. Aortic pulse wave velocity evaluated by 4D flow MRI across the adult lifespan. J Magn Reson Imaging 2022;56(2):464–473.
84. Dushfunian D, Maroun A, Berhan H, et al. Robustness of 4D flow MRI derived aortic wall shear stress and pulse wave velocity across different protocols in healthy controls and in patients with bicuspid aortic valve. Int J Cardiovasc Imaging 2025;41(1):137–149.
85. Dyverfeldt P, Trenti C, Ziegler M, Bjarnegård N, Lindenberger M. Helical flow in tortuous aortas and its relationship to turbulence: A whole-aorta 4D flow MRI study. Front Cardiovasc Med 2023;10:1124604.
86. Ha H, Ziegler M, Welander M, et al. Age-related vascular changes affect turbulence in aortic blood flow. Front Physiol 2018;9:36.
87. Tyagi S, Safal S, Tyagi D. Aortitis and aortic aneurysm in systemic vasculitis. Indian J Thorac Cardiovasc Surg 2019;35(Suppl 2):47–56.
88. Álvarez Vázquez A, López Alcolea J, Urmeneta Ulloa J, et al. Takayasu's arteritis causing coronary stenosis with myocardial ischemia, severe aortic regurgitation, and pericarditis. Radiol Case Rep 2025;20(1):791–796.
89. Zhang N, Pan L, Liu J, et al. Comparison of Different Thoracic Aortic Wall Characteristics for Assessment of Disease Activity in Takayasu Arteritis: A Quantitative Study with 3.0 T Magnetic Resonance Imaging. Rev Cardiovasc Med 2022;23(3):92.
90. Riambau V, Böckler D, Brunkwall J, et al. Editor's Choice - Management of Descending Thoracic Aorta Diseases: Clinical Practice Guidelines of the European Society for Vascular Surgery (ESVS). Eur J Vasc Endovasc Surg 2017;53(1):4–52.
91. Hope TA, Zarins CK, Herfkens RJ. Initial experience characterizing a type I endoleak from velocity profiles using time-resolved three-dimensional phase-contrast MRI. J Vasc Surg 2009;49(6):1580–1584.
92. Rengier F, Delles M, Weber TF, et al. In vitro validation of flow measurements in an aortic nitinol stent graft by velocity-encoded MRI. Eur J Radiol 2011;80(1):163–167.
93. Bunck AC, Jüttner A, Kröger JR, et al. 4D phase contrast flow imaging for in-stent flow visualization and assessment of stent patency in peripheral vascular stents–a phantom study. Eur J Radiol 2012;81(9):e929–e937.
94. Righini P, Secchi F, Mazzaccaro D, et al. Four-Dimensional Flow MRI for the Evaluation of Aortic Endovascular Graft: A Pilot Study. Diagnostics (Basel) 2023;13(12):2113.
95. Cosset B, Boussel L, Davila Serrano E, et al. Hemodynamic Changes Before and After Endovascular Treatment of Type B Aortic Dissection by 4D Flow MRI. Front Cardiovasc Med 2022;9:873144.
96. Sakata M, Takehara Y, Katahashi K, et al. Hemodynamic Analysis of Endoleaks After Endovascular Abdominal Aortic Aneurysm Repair by Using 4-Dimensional Flow-Sensitive Magnetic Resonance Imaging. Circ J 2016;80(8):1715–1725.
97. Katahashi K, Sano M, Takehara Y, et al. Flow dynamics of type II endoleaks can determine sac expansion after endovascular aneurysm repair using four-dimensional flow-sensitive magnetic resonance imaging analysis. J Vasc Surg 2019;70(1):107–116.e1.
98. Lenz A, Petersen J, Riedel C, et al. 4D flow cardiovascular magnetic resonance for monitoring of aortic valve repair in bicuspid aortic valve disease. J Cardiovasc Magn Reson 2020;22(1):29.
99. Keller EJ, Malaisrie SC, Kruse J, et al. Reduction of aberrant aortic haemodynamics following aortic root replacement with a mechanical valved conduit. Interact Cardiovasc Thorac Surg 2016;23(3):416–423.
100. Bissell MM, Loudon M, Hess AT, et al. Differential flow improvements after valve replacements in bicuspid aortic valve disease: a cardiovascular magnetic resonance assessment. J Cardiovasc Magn Reson 2018;20(1):10.
101. Kamada H, Ota H, Nakamura M, et al. Perioperative Hemodynamic Changes in the Thoracic Aorta in Patients With Aortic Valve Stenosis: A Prospective Serial 4D-Flow MRI Study. Semin Thorac Cardiovasc Surg 2020;32(1):25–34.
102. Bollache E, Fedak PWM, van Ooij P, et al. Perioperative evaluation of regional aortic wall shear stress patterns in patients undergoing aortic valve and/or proximal thoracic aortic replacement. J Thorac Cardiovasc Surg 2018;155(6):2277–2286.e2.
103. Semaan E, Markl M, Malaisrie SC, et al. Haemodynamic outcome at four-dimensional flow magnetic resonance imaging following valve-sparing

aortic root replacement with tricuspid and bicuspid valve morphology. Eur J Cardiothorac Surg 2014;45(5):818–825.
104. Collins JD, Semaan E, Barker A, et al. Comparison of Hemodynamics After Aortic Root Replacement Using Valve-Sparing or Bioprosthetic Valved Conduit. Ann Thorac Surg 2015;100(5):1556–1562.
105. Farag ES, Vendrik J, van Ooij P, et al. Transcatheter aortic valve replacement alters ascending aortic blood flow and wall shear stress patterns: A 4D flow MRI comparison with age-matched, elderly controls. Eur Radiol 2019;29(3):1444–1451.
106. Rooijakkers MJP, El Messaoudi S, Stens NA, et al. Assessment of paravalvular regurgitation after transcatheter aortic valve replacement using 2D multi-velocity encoding and 4D flow cardiac magnetic resonance. Eur Heart J Cardiovasc Imaging 2024;25(7):929–936.
107. Berhane H, Scott M, Elbaz M, et al. Fully automated 3D aortic segmentation of 4D flow MRI for hemodynamic analysis using deep learning. Magn Reson Med 2020;84(4):2204–2218.
108. Berhane H, Scott MB, Barker AJ, et al. Deep learning–based velocity antialiasing of 4D-flow MRI. Magn Reson Med 2022;88(1):449–463.
109. Bustamante M, Viola F, Engvall J, Carlhäll CJ, Ebbers T. Automatic time-resolved cardiovascular segmentation of 4D flow MRI using deep learning. J Magn Reson Imaging 2023;57(1):191–203.
110. Marin-Castrillon DM, Geronzi L, Boucher A, et al. Segmentation of the aorta in systolic phase from 4D flow MRI: multi-atlas vs. deep learning. MAGMA 2023;36(5):687–700.
111. Villié A, Schmitter S, von Saldern JGR, Demange S, Oberleithner K. Physics-informed neural networks for enhancing medical flow magnetic resonance imaging: Artifact correction and mean pressure and Reynolds stresses assimilation. Phys Fluids 2025;37(2):025194.
112. Ericsson L, Hjalmarsson A, Akbar MU, et al. Generalized Super-Resolution 4D Flow MRI - Using Ensemble Learning to Extend Across the Cardiovascular System. IEEE J Biomed Health Inform 2024;28(12):7239–7250.
113. Levilly S, Moussaoui S, Serfaty JM. Segmentation-Free Velocity Field Super-Resolution on 4D Flow MRI. IEEE Trans Image Process 2024;33:5637–5649.
114. Callmer P, Bonini M, Ferdian E, et al. Deep learning for temporal super-resolution 4D Flow MRI. arXiv 2025. Preprint posted online January 15, 2025; doi:10.48550/arxiv.2501.08780.
115. Berhane H, Maroun A, Dushfunian D, et al. Anatomy-derived 3D Aortic Hemodynamics Using Fluid Physics-informed Deep Learning. Radiology 2025;315(2):e240714.
116. Vishnevskiy V, Walheim J, Kozerke S. Deep variational network for rapid 4D flow MRI reconstruction. Nat Mach Intell 2020;2(4):228–235.
117. Jacobs L, Piccirelli M, Vishnevskiy V, Kozerke S. FlowMRI-Net: A Generalizable Self-Supervised 4D Flow MRI Reconstruction network. arXiv 2024. Preprint posted online October 11, 2024; doi:10.48550/arxiv.2410.08856.
118. Kim D, Jen ML, Eisenmenger LB, Johnson KM. Accelerated 4D-flow MRI with 3-point encoding enabled by machine learning. Magn Reson Med 2023;89(2):800–811.
119. Yinghui W, Haonan X, Jing W, et al. Artificial intelligence in four-dimensional imaging for motion management in radiation therapy. Artif Intell Rev 2025;58(4):103.
120. Shan Y, Li J, Wang Y, et al. Aortic shear stress in patients with bicuspid aortic valve with stenosis and insufficiency. J Thorac Cardiovasc Surg 2017;153(6):1263–1272.e1.
121. van Ooij P, Markl M, Collins JD, et al. Aortic valve stenosis alters expression of regional aortic wall shear stress: New insights from a 4-dimensional flow magnetic resonance imaging study of 571 subjects. J Am Heart Assoc 2017;6(9):e005959.
122. Shan Y, Li J, Wang Y, et al. Aortic stenosis exacerbates flow aberrations related to the bicuspid aortic valve fusion pattern and the aortopathy phenotype. Eur J Cardiothorac Surg 2019;55(3):534–542.
123. Weiss EK, Jarvis K, Maroun A, et al. Systolic reverse flow derived from 4D flow cardiovascular magnetic resonance in bicuspid aortic valve is associated with aortic dilation and aortic valve stenosis: a cross sectional study in 655 subjects. J Cardiovasc Magn Reson 2023;25(1):3.
124. Allen BD, Kilinc O, Pradella M, et al. Entry Tear Hemodynamics Detect Patients With Adverse Aorta-Related Outcomes in Type B Aortic Dissection. JACC Cardiovasc Imaging 2023;16(5):711–712.
125. Engel J, Kilinc O, Weiss E, et al. Interval changes in four-dimensional flow-derived in vivo hemodynamics stratify aortic growth in type B aortic dissection patients. J Cardiovasc Magn Reson 2024;26(2):101078.
126. Desai L, Stefek H, Berhane H, Robinson J, Rigsby C, Markl M. Four-Dimensional flow Magnetic Resonance Imaging for Assessment of Pediatric Coarctation of the Aorta. J Magn Reson Imaging 2022;55(1):200–208.
127. Rengier F, Delles M, Eichhorn J, et al. Noninvasive 4D pressure difference mapping derived from 4D flow MRI in patients with repaired aortic coarctation: comparison with young healthy volunteers. Int J Cardiovasc Imaging 2015;31(4):823–830.
128. Geiger J, Hirtler D, Gottfried K, et al. Longitudinal Evaluation of Aortic Hemodynamics in Marfan Syndrome: New Insights from a 4D Flow Cardiovascular Magnetic Resonance Multi-Year Follow-Up Study. J Cardiovasc Magn Reson 2017;19(1):33.